



Fluor-carbonated hydroxyapatite coatings by pulsed laser deposition to promote cell viability and antibacterial properties

Bettiana Marcela Hidalgo-Robatto^a, John Jairo Aguilera-Correa^b, Miriam López-Álvarez^{a,*}, David Romera^b, Jaime Esteban^b, Pío González^a, Julia Serra^a

^a New Materials Group, Department of Applied Physics, University of Vigo, IISGS, MTI, Campus Lagoas-Marcosende, 36310 Vigo, Spain

^b Department of Clinical Microbiology, IIS Jiménez Díaz Foundation, Autonomous University of Madrid, Madrid, Spain



ARTICLE INFO

Keywords:

Fluor-hydroxyapatite coatings
Marine bioceramics
Pulsed laser deposition
Antibacterial properties
ALP synthesis

ABSTRACT

Fluorine, an essential element present in bone and dental tissues, promotes mineralization and is directly involved in the bone formation process. The antibacterial effects of fluorine on oral bacteria are also well known. In this study, metallic implants were coated with a thin layer of calcium phosphate enriched with fluorine to improve osteointegration and protect against infections. These coatings were obtained by pulsed laser deposition (PLD) using, as a target, a bioceramic of marine origin, mainly composed of fluorapatite from the enameloid of shark teeth. The compositional dependence of coatings on H₂O vapor pressures applied during PLD was analyzed in order to optimize physicochemical properties. Physicochemical characterization to evaluate morphology (SEM), thickness (interferometric profilometry), structure (XRD) and composition (FTIR, XPS) was performed. To evaluate the biological response, both MC3T3-E1 pre-osteoblasts and bacterial strains *Staphylococcus aureus* and *Staphylococcus epidermidis*, most responsible for 77% of infections associated with prosthetic implants, were tested. Proper cell proliferation (MTT assay) and ALP synthesis up to 21 days were confirmed. Antibacterial properties were also demonstrated: compared to synthetic hydroxyapatite coatings, there was a significant reduction in colony-forming units (CFUs) for both strains.

1. Introduction

Fluorine (F) is an essential element present in bone and dental tissues. It is thought to be an enhancer of the synthesis of bone cell growth factors, acting primarily on the osteoprogenitor cells and/or undifferentiated osteoblasts cells rather than on highly differentiated osteoblasts. It is therefore related to the promotion of mineralization and is directly involved in the bone formation process [1]. Fluorine contributes to bone healing and regeneration by inducing the differentiation of osteoprogenitor and undifferentiated precursor cells into osteoblasts [2]. Moreover, in the form of fluorapatite, it contributes to the development of a highly crystalline and stable apatite [3], with improved mechanical properties in relation to geological hydroxyapatite, with good stiffness, high elastic modulus and hardness.

The antibacterial effects of fluorine in the form of fluoride on oral bacteria are also well known [4]. There is evidence that fluoride can interfere with enzyme activity and reduce acid production by oral bacteria (both Gram-positive and Gram-negative), thereby inhibiting the enrichment of cariogenic species within dental plaque [5, 6]. The

capacity of fluorine (released from a cement) to inhibit the metabolism of certain bacteria (i.e., oral streptococci) has previously been reported [7]. Studies suggest that fluoride also has anti-plaque properties. It is well documented that amine fluoride and stannous fluoride possess bactericidal properties against oral bacteria [8, 9]. The pre-incubation of hydroxyapatite with amine fluoride significantly decreases the viability of *Streptococcus sobrinus* in biofilm, whereas sodium fluoride or chlorhexidine does not [10].

Joint prostheses are one of the most important medical advances made to date due to their ability to relieve joint pain, restore joint function, and allow millions of patients around the world to recover their independence [11]. However, these prostheses are liable to failure, the main causes being aseptic loosening, infection, dislocation, and fracture of the prosthesis or bone [12]. Aseptic loosening in particular can occur through loss of fixation caused by a lack of initial tissue-implant fixation, leading to a mechanical loss over time and/or particle-induced osteolysis around the implant [13]. Therefore, if osteointegration were promoted, aseptic loosening could be prevented [14].

* Corresponding author.

E-mail addresses: bhidalgo@uvigo.es (B.M. Hidalgo-Robatto), john.aguilera@fdj.es (J.J. Aguilera-Correa), miriammsd@uvigo.es (M. López-Álvarez), david.romerag@quironsalud.es (D. Romera), jaim.e Esteban@uam.es (J. Esteban), pglez@uvigo.es (P. González), jserra@uvigo.es (J. Serra).

<https://doi.org/10.1016/j.surfcoat.2018.06.047>

Received 30 April 2018; Received in revised form 12 June 2018; Accepted 22 June 2018

Available online 27 June 2018

0257-8972/ © 2018 Elsevier B.V. All rights reserved.

Osteointegration can be promoted by covering prostheses with a calcium phosphate layer, mimicking the inorganic composition of bone [14]. Applying such a layer to the surface of titanium implant devices has been proven to enhance bone formation around the implants and contribute to cementless fixation, improving clinical success at an early stage after implantation [15]. Plasma-spray was the first technique used to produce calcium phosphate coatings on dental root implants and hip and knee orthopedic prostheses. However, the high thickness of the coatings (50–200 μm , limitation of the technique) resulted in their partial disappearance during the implantation time, causing the proliferation of macrophages. The pulsed laser deposition (PLD) technique, on the other hand, produces thin coatings with good adhesion properties; it also allows the precise control of the chemistry and crystallinity of the coatings [16, 17]. Synthetic carbonated hydroxyapatite (HA) coatings produced by PLD have been successfully tested, showing enhanced or similar osteointegration to their plasma-sprayed equivalents, but with improved adhesion properties, without the risk of delamination or detachment of the coating [18–25].

Prosthetic joint infection occurs infrequently (1–2% of all cases), though it is a devastating complication with high morbidity and substantial costs. The economic burden of prosthetic joint infection is expected to grow in the coming years due to the increase in patients undergoing arthroplasty replacements [26]. Gram-positive cocci, the most common of which are *Staphylococcus aureus* and *Staphylococcus epidermidis*, represent up to 77% of all infections [27–31].

Apart from the administration of oral or intravenous antibiotics to prevent bacterial colonization, the local action of different chemical elements incorporated in trace concentrations into the calcium phosphate structure has been investigated. HA coatings doped with Se, Ag, Cu or Zn have been proven to reduce bacterial biofilm formation due to the chemical changes they promote in the cellular environment [18, 20–23, 32].

Given the interesting properties of fluorine, this paper will describe the use of PLD to coat metallic implants with a thin layer of bioceramic of marine origin, mainly composed of fluorapatite obtained from the enameloid of shark teeth. It will evaluate the structure and composition of different coatings obtained at various H_2O vapor pressures. The vapor pressure exercise examines the dependence of the coatings on pressure, to guarantee optimal properties and good transference from the original bioceramic. Finally, the proliferation and alkaline phosphatase (ALP) synthesis of MC3T3-E1 pre-osteoblasts on the fluor-carbonated HA coatings, together with their antibacterial properties against *Staphylococcus aureus* and *Staphylococcus epidermidis* strains, will be discussed.

2. Materials and methods

2.1. Coating process

Following the same methodology as previous studies [33–36], the fluor-carbonated HA coatings were processed using a UV ArF* excimer laser ($\lambda = 193 \text{ nm}$) source (Lambda Physik COMPEX 205). PLD targets with a mass of 2 g and a diameter of 20 mm were prepared using a bioceramic, developed in our laboratories, obtained from the enameloid of shark teeth (*Isurus oxyrinchus* and *Prionace glauca* species) [37, 38]. The bioceramic granulate was compacted by raising the pressure to 8 tons and repeating the process three times; the targets were then sintered at 1260 $^\circ\text{C}$ to improve their consistency. They were irradiated for up to 120 min to obtain different thicknesses, using in all cases a pulse frequency of 10 Hz and an energy density of 3.2 J/cm². Substrates were maintained at a temperature of 460 $^\circ\text{C}$. Coatings of synthetic hydroxyapatite (Plasma Biotol Captal-R) were also prepared at 0.45 mbar to be used as reference material, labeled as Ref-HA coatings.

The fluor-carbonated HA coatings, labeled as Bio-FHA, were deposited on titanium alloy (Ti₆Al₄V) discs with dimensions of 4.8 mm diameter and 1 mm thickness. Before being placed inside the PLD

vacuum chamber, the substrates were cleaned by 7-minute sonication cycles using 5% nitric acid, methanol or acetone, interspersed by cycles of rinsing in distilled water. Prior to deposition, the chamber atmosphere was lowered to a pressure of 10^{−4} mbar and subsequently filled with a H_2O vapor atmosphere, varying the pressures as follows: 0.0, 0.15, 0.25, 0.35 and 0.45 mbar.

2.2. Physicochemical characterization

The morphology of the coatings was analyzed by scanning electron microscopy (SEM) using a JEOL JSM-6700F microscope. Interferometric profilometry was used to determine the thickness mean values of the different coatings. Three profiles per condition (coating type on silicon as substrate due to technical requirements) were measured in a non-contact high resolution optical profilometer (WYKO NT-1100). Structural and compositional measurements were taken by Fourier transform infrared spectroscopy (FTIR, Bruker IFS-28) in the range of 550 to 5000 cm^{−1}, using silicon as substrate due to technical requirements; X-ray diffraction (XRD, Siemens D-5000 Diffractometer); and X-ray photoelectron spectroscopy (XPS, Thermo Scientific K-ALPHA ESCA). All these measurements were performed on the complete series of coatings at different H_2O vapor pressures in order to evaluate the dependence of physicochemical properties on variations in pressure.

The bioceramic target had previously been characterized [36–38]; a semi-quantitative evaluation established the main contribution as a 91% apatitic phase of fluorapatite (Ca₅(PO₄)₃F). The XRD typical reflections were located at 21.8, 22.9, 25.8, 28.1, 29.0, 31.9, 32.2, 33.0 and 34.1 $^\circ$, corresponding respectively to the (2,0,0), (1,1,1), (0,0,2), (1,0,2), (2,1,0), (1,2,1), (1,1,2), (3,0,0) and (2,0,2) diffraction planes [39, 40]. The 9% non-apatitic phase was attributed to tricalcium bis (orthophosphate), Ca₃O₈P₂, and/or whitlockite, Ca₁₈Mg₂H₂(PO₄)₁₄, with typical reflections at 27.84 and 31.16 $^\circ$, corresponding respectively to the (2,0,8) and (0,2,10) diffraction planes [41]. In relation to its composition (XPS), electronic transitions associated with the main elements of calcium phosphate bioceramics (Ca_{2p} and P_{2p}) and other minority elements (F_{1s}, Na_{1s} and Mg_{1s}) were quantified (in at.%) as 16.93, 14.16, 2.09, 2.75 and 1.40, respectively. The binding energy (BE) at 684.66 eV corresponded to F_{1s}. According to the literature [42], a binding energy of 684.20 eV indicates that fluoride ions are incorporated into the HA lattice structure. A slightly higher value was obtained in our target due to the charge correction process.

2.3. Biological characterization: response of pre-osteoblastic cells

Bio-FHA and Ref-HA coatings obtained at 0.45 mbar were subjected to gamma sterilization and incubated with the pre-osteoblastic cell line MC3T3-E1 (ECACC, catalog No.: 99072810). Cells were regularly cultured in alpha minimum essential medium (α -MEM Lonza) supplemented with 10% (vol/vol) of fetal bovine serum (FBS, Invitrogen) and with a 2% combination of amphotericin B, penicillin and streptomycin (Invitrogen, catalog 15,240–062), at 37 $^\circ\text{C}$ and 5% of CO₂ in a humidified atmosphere. Four replicates were evaluated per coating and per condition. Tissue culture polystyrene (TCP) was used as a control experiment for the healthy stage of cells. The culture medium was renewed every 2 to 3 days.

2.4. Cell morphology

Cell morphology on the coatings was evaluated by SEM and confocal laser scanning microscopy (CLSM), with a direct seeding of 100 μl of cell suspension 1.7 $\times 10^5$ cells/ml in 96-well tissue culture microplates. For SEM evaluation after 7 and 21 days of incubation, the culture medium was removed and cells were fixed with 2.5% glutaraldehyde solution in phosphate buffered saline (PBS, Lonza) for 2 h at 4 $^\circ\text{C}$. Samples were washed three times for 30 min each with PBS. After

fixation, they were subjected to dehydration by replacing the PBS with a graded series of ethanol (10, 20, 30, 40, 50, 60, 70, 80, 90 and 100%) for 30 min each. The process was followed by a chemical dehydration series of 100% ethanol and hexamethyldisilazane (HMDS, Ted Pella, USA) at concentrations of 25, 50 and 75% for 15 min each, ending with immersion in 100% HMDS for 30 min. Finally, the coatings were left to dry overnight and were affixed to aluminum stubs for examination via SEM Philips XL30. The cytoskeleton was evaluated by CLSM (Bio-Rad MRC 1024) after 20 days of culture. At that time, cells were fixed with 4% paraformaldehyde solution for 10 min at room temperature, after which they were permeabilized for 5 min with 0.1% (vol/vol) Triton X-100 in PBS buffer $1 \times$. Alexa Fluor 488 phalloidin solution was added for 20 min in darkness in order to visualize actin filaments. After incubation, cell nuclei were labeled with propidium iodide solution for 5 min in darkness.

2.5. Cell proliferation

To evaluate their proliferation, cells were first directly seeded on the coatings and incubated with a volume of 100 μ l of cell suspension 1.7×10^5 cells/ml in 96-well tissue culture microplates. Using new 96-well tissue culture microplates, proliferation was then quantified after incubation periods of 7 and 21 days using the methyl thiazol tetrazolium method (MTT assay, Roche); the tetrazolium component in living cells is reduced by mitochondrial into a purple formazan product. After overnight incubation, samples were removed and the resulting colored solution quantified as optical density values using a Bio-Rad Model 550 microplate spectrophotometer. These data were normalized per cm^2 due to the different areas of coatings and TCP controls.

2.6. Cell differentiation

Cell differentiation of osteoblasts was determined after 7 and 21 days using the Alkaline Phosphatase (ALP) Assay Kit (Abcam), an early osteogenic differentiation marker. To induce differentiation 1 day after seeding, ascorbic acid 2-phosphate (Sigma-Aldrich, 2 mM) and glycerol 2-phosphate (Sigma-Aldrich, 10 mM) were added to the α -MEM medium. In order to obtain cell lysates, discs were carefully rinsed three times with PBS (Lonza) and subjected to osmotic and thermal shocks with sterile ultrapure water. Using a Bio-Rad Model 550 microplate spectrophotometer, cell lysates were then used to quantify the activity of the ALP enzyme using the spectrophotometric assay based on the conversion of *p*-nitrophenyl-phosphate to *p*-nitrophenol.

2.7. Biological characterization: response of bacterial strains

To perform the experiment, strains of *Staphylococcus aureus* 15981 (*S. aureus*) and *Staphylococcus epidermidis* 35984 (*S. epidermidis*) were used on the Bio-FHA and Ref-HA coatings that had previously been placed in a 96-well plate (Thermo Fisher Scientific, Massachusetts, USA). Biofilms of each species were formed by transferring to the coatings 200 μ l containing 10^6 colony forming units of each strain per ml (CFU/ml of initial concentration), incubated in tryptic soy broth (Biomérieux, Marcy-l'Étoile, France) and supplemented with 1% glucose. After 24 h of incubation at 37 °C and 5% CO_2 , the medium was removed and samples were washed three times with 200 μ l 0.9% NaCl sterile saline (B. Braun, Melsungen, Germany). Biofilms were disrupted by sonication with an Ultrasons-H 3000840 low-power bath sonicator (J. P. Selecta, Barcelona, Spain) at 22 °C for 5 min [39]. The CFU/ cm^2 values were estimated by the drop plate method [40]. These assays were performed in triplicate.

A morphological evaluation of the biofilms was also carried out after 24 h; they were fixed using glutaraldehyde (2.5%) in sodium cacodylate buffer (0.1 M) at pH 7 at room temperature for 2 h. After fixation, samples were subjected to dehydration by replacing the buffer with a graded series of ethanol (30, 50, 70, 90 and 100%) for 10 min

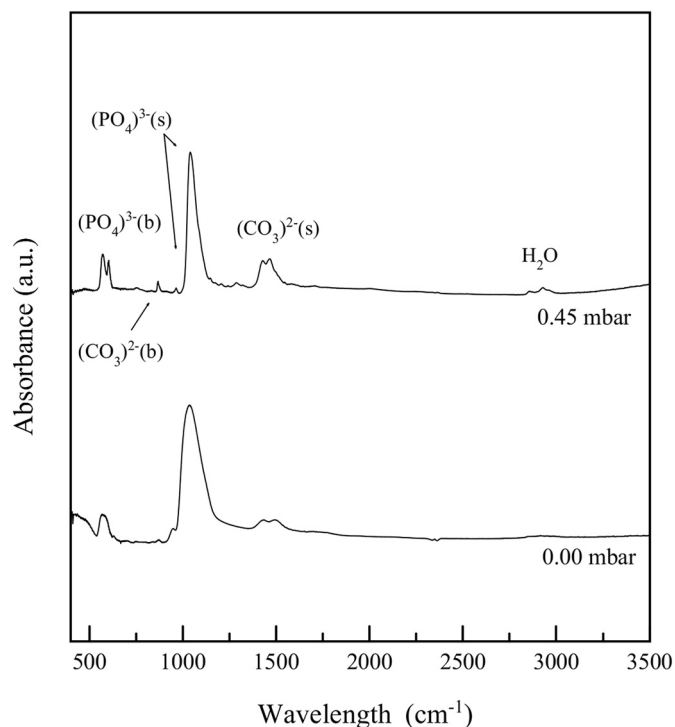


Fig. 1. FTIR spectra of Bio-FHA coatings deposited at H_2O vapor pressures of 0.00 and 0.45 mbar during the PLD process.

each at room temperature. Finally, the biofilms were left to dry overnight, affixed to aluminum stubs and coated with platinum using a Bal-Tec MED020, for SEM analysis in JEOL JSM-6700 equipment.

2.8. Statistical analysis

Data on the pre-osteoblasts are presented as mean values \pm standard error of the mean. Statistical differences were evaluated using SPSS Statistics (vs. 23.0). In all cases, the significance level was set at 0.05. Each data element was analyzed using the non-parametric Mann-Whitney *U* test. The statistical analysis of bacterial strains was performed using the non-parametric unilateral Wilcoxon's test with a statistical significance level of 0.05. The microbiological data are presented as median and interquartile range.

3. Results and discussion

3.1. Coating characterization: dependence on H_2O vapor pressure

The FTIR spectra of the Bio-FHA coatings deposited at H_2O vapor pressures of 0.45 and 0.0 mbar are presented in Fig. 1. The main vibration modes were identified using previous literature [24, 46–53] as follows: (i) phosphate groups with a strong peak located between 1000 and 1200 cm^{-1} attributed to the asymmetric stretching of P–O bonds, a weak band at 950 cm^{-1} due to symmetric stretching and an absorption band between 550 and 600 cm^{-1} attributed to symmetric bending; (ii) carbonate groups with an absorption band between 1400 and 1500 cm^{-1} attributed to the asymmetric stretching of C–O bonds and a weaker band at 870 cm^{-1} due to asymmetric bending; and (iii) adsorbed water with a characteristic broad band around 3000 cm^{-1} .

The results indicate that at all pressures the bond structure of the coatings was basically a calcium phosphate. However, differences were observed as the H_2O vapor pressure varied. As the vapor pressure increased, the intensity of carbonate bands also increased; the $[\text{CO}_3^{2-}(\text{s})/\text{PO}_4^{3-}(\text{s})]$ ratio was 30% higher in the Bio-FHA coating deposited at 0.45 mbar than at 0.00 mbar. At the same time, the full width at half

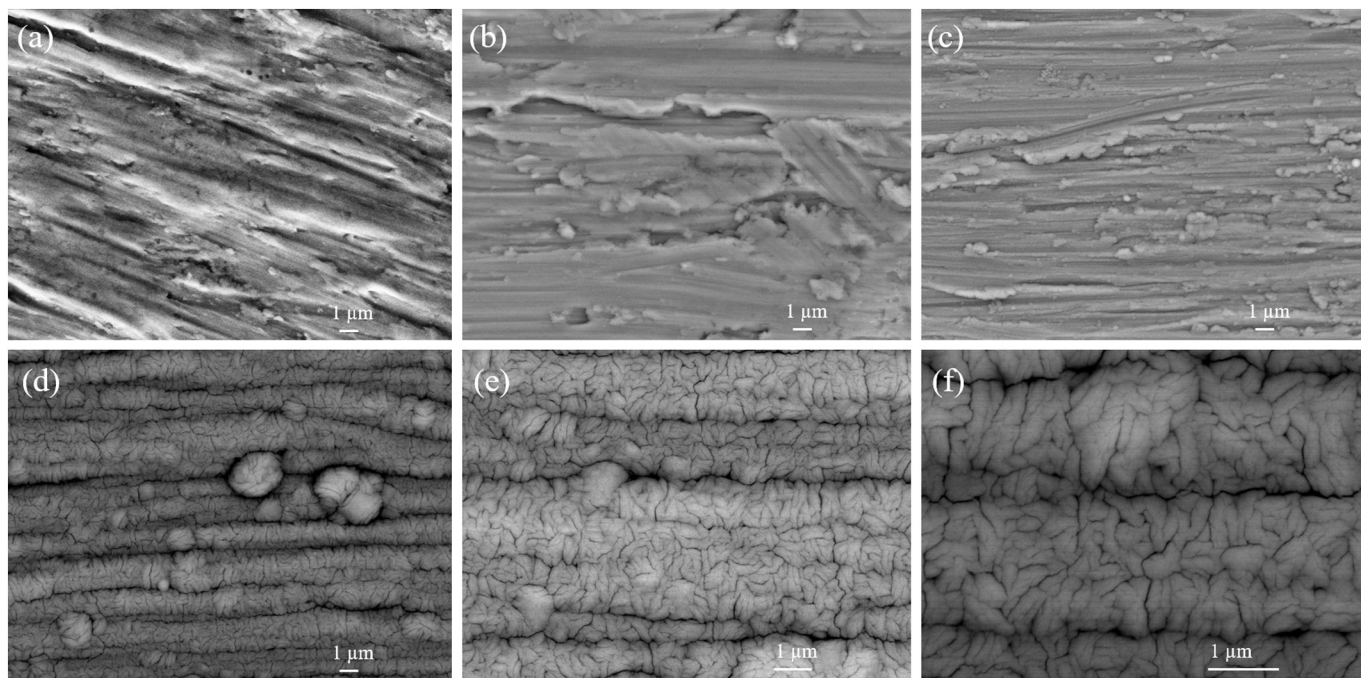


Fig. 2. SEM micrographs of processed titanium alloy substrate (a), the Bio-FHA coatings at 0.00 mbar for 30 min (b), at 0.45 mbar for 30 min (c), and at 0.45 mbar for 120 min (d–f). Magnifications of 5000 \times (a–d), 10,000 \times (e), 20,000 \times (f).

maximum (FWHM) of the main peak of PO_4^{3-} groups (asymmetric stretching) decreased by about 70% for the Bio-FHA coating deposited at 0.45 mbar than at 0.00 mbar. A better definition of the PO_4^{3-} bending band was also observed, indicating that the short-range order in the structure was enhanced.

Morphology was analyzed by SEM and results are displayed in Fig. 2: a micrograph of the surface of the processed titanium alloy substrate (a), the Bio-FHA coatings processed at 0.00 mbar for 30 min (b), at 0.45 mbar for 30 min (c) and at 0.45 mbar for 120 min at three magnifications (d–f). As can be seen, the surface morphology of the tested coatings was composed of aggregates of globular shape, typical of a HA film (b–f). Moreover, coatings grew following the topography of the processed substrate (a). For the coating deposited at 0.45 mbar for 120 min (d–f), globular morphology with ridges and valleys following the direction of the topography of the processed titanium substrates can be clearly observed (d). Increased magnifications (10,000 \times and 20,000 \times) revealed that the coating was composed of elongated structures of < 1 μm in length (e) and (f).

Evidence provided by the FTIR analysis and the SEM evaluation, confirming the presence of phosphate groups and the typical globular morphology of calcium phosphate, agreed with previous studies that have obtained coatings by the same technique [20, 24, 34, 50, 53, 54]. The elongated structures of < 1 μm in length observed in the present study could potentially be attributed to the aligned faceted crystals already described by Lopez-Alvarez et al. These crystals, of approx. 0.5–1.0 μm in one dimension and 4–10 μm in the others, are part of the shark enameloid structure [37, 38] where fluorine is present in the bioceramic [36–38].

The thickness value obtained by interferometric profilometry for the Bio-FHA coatings deposited at 0.45 mbar of H_2O vapor pressure for 30 min was $0.11 \pm 0.01 \mu\text{m}$, while for those processed at 0.00 mbar the value was $0.54 \pm 0.05 \mu\text{m}$. The deposit rate was 3.5 nm/min for the coatings processed at 0.45 mbar, and 18.1 nm/min for those processed at 0.00 mbar. These results indicate that increased H_2O vapor pressure diminishes the thickness of the coatings. The thicknesses obtained in both conditions were much lower than the profile of the processed titanium alloy substrates, which is why both coatings adapt perfectly to the substrate topography without modifying it.

The crystallinity of the coatings was analyzed by XRD. A defined crystalline structure with clear, sharp and intense peaks was found for the coatings deposited above 0.25 mbar. For the coatings deposited below this H_2O vapor pressure, the spectra revealed the presence of a unique wide band. Fig. 3 depicts XRD spectra in the range of 20 to 35 $^\circ$ for the Bio-FHA coatings deposited at 0.45 and 0.00 mbar. As can be seen, Bio-FHA coatings processed at 0.45 mbar reveal the typical reflections associated with apatite structures, such as hydroxyapatite $\text{Ca}_5(\text{PO}_4)_3(\text{OH})$, carbonated-hydroxyapatite or fluorapatite $\text{Ca}_5(\text{PO}_4)_3\text{F}$, located at 29.4, 32.1 and 33.4 $^\circ$, corresponding respectively to the (2,1,0), (1,1,2) and (3,0,0) diffraction planes [20, 41, 46, 49, 53, 55–58].

For a more detailed analysis, the diffraction peak at plane (1,1,2) was selected to estimate the crystallite size (τ) on the processed coatings at different H_2O vapor pressures using the Scherrer equation (1):

$$\tau = K \lambda / B \cos \theta \quad (1)$$

where λ is the wavelength of the incident radiation, θ is the Bragg angle and B is the FWHM of the peak intensity corresponding to the (1,1,2) reflection. The single-crystal sizes obtained were 65 nm for the Bio-FHA coatings processed at 0.45 mbar, and 17 nm at 0.00 mbar; the values for 0.35, 0.25 and 0.15 mbar were 48, 43 and 20 nm respectively. Crystallite size therefore increases as H_2O vapor pressure increases, meaning that the crystallinity of these coatings can be modified depending on the pre-defined pressure.

These results were in good agreement with those obtained in the FTIR analysis (Fig. 2), where defined bands were also observed with the progressive incorporation of H_2O vapor pressure. It is well known that a HA structure needs OH ions to stabilize its crystalline structure. In the PLD process, the presence of a H_2O vapor atmosphere reduces the kinetic energy of the species (which could influence the deposit rate, promoting a decrease in thickness), enhancing the crystalline quality of the films [16]. It is also well known [43, 44] that the water forms a ternary equilibrium with the CaO and P_2O_5 groups. Phase diagrams of CaO and P_2O_5 show the reactivity of calcium orthophosphates with humidity at high temperatures, following reactions such as:

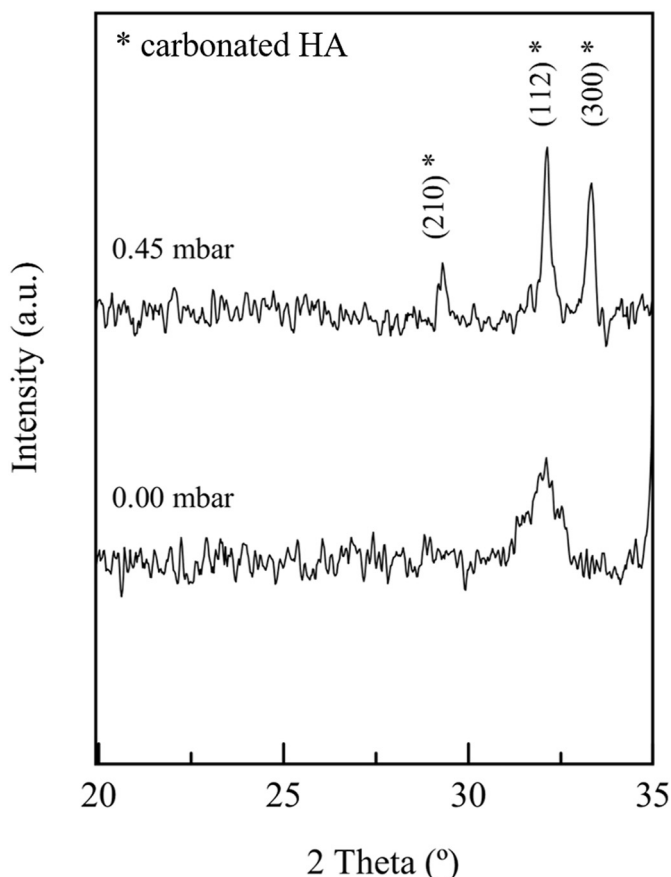
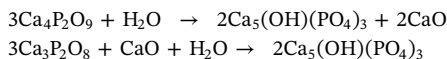


Fig. 3. XRD patterns of Bio-FHA coatings deposited at H₂O vapor pressures of 0.45 and 0.00 mbar during the PLD process.



When the crystalline structures of the ablation target were compared with those obtained for the coatings, the presence of diffraction planes—(2,1,0), (1,1,2) and (3,0,0)—on the Bio-FHA coatings processed at 0.45 mbar (and also at 0.25 and 0.35 mbar) confirmed the efficient material transference from the target to the coatings. It is worth highlighting that the single-crystal size of 65 nm estimated for the Bio-FHA coatings processed at 0.45 mbar was close to that reported for the original bioceramic of pyrolyzed shark enameloid (60 nm) [36].

Finally, the compositional analysis performed by XPS enabled the identification and atomic percentage quantification of the elements present in the Bio-FHA coatings. As can be seen from the quantitative evaluation in Table 1, the chemical composition of the whole series of Bio-FHA coatings was based on Ca, P and also F, with the incorporation of Na for pressures ≥ 0.25 mbar, and of Mg at the highest tested pressure (0.45 mbar).

Table 1
Atomic percentages of main elements of Bio-FHA coatings processed at H₂O vapor pressures of 0.00 to 0.45 mbar determined by XPS.

Bio-FHA coatings	Composition (at.%)					Ca/P ratio	
	Ca _{2p}	P _{2p}	F _{1s}	Na _{1s}	Mg _{1s}		
Vapor pressure (mbar)	0.45	17.98	9.89	1.96	0.95	0.86	1.82
	0.35	17.48	9.92	2.28	0.55	–	1.76
	0.25	15.14	7.63	1.33	1.06	–	1.98
	0.15	15.76	4.13	1.17	–	–	3.82
	0.00	17.39	5.02	1.28	–	–	3.46

When the composition of the ablation target (shown in Materials and Methods section) was compared with that of the coatings, it was found that the five elements were successfully transferred only in the Bio-FHA coatings processed at 0.45 mbar. In other words, higher H₂O vapor pressures during the PLD processing favored the incorporation of Ca, P and F, as well as minority elements (Na, Mg). It is interesting to note that the coatings deposited at 0.35 and 0.45 mbar of H₂O vapor pressure presented a Ca/P ratio of around 1.8, whereas it was 1.2 in the case of the ablation target. The Ca/P ratio therefore approaches that of sintered synthetic carbonated hydroxyapatite, Ca/P = 1.7 [16], when the pressure is increased to 0.35–0.45 mbar. The same tendency of lower Ca/P ratios with higher pressures has already been reported for synthetic calcium phosphate coatings obtained by PLD at 0.15 to 0.80 mbar, explained by the fact that more phosphorus can be retained in the coating [16]. In the same way as the crystalline structure, the composition is also affected by the H₂O vapor pressure used. During the PLD process, this atmosphere facilitates the control of film stoichiometry by promoting a hydration reaction between the film species and H₂O or its decomposition products.

High-resolution XPS spectra of the F_{1s} electronic transition for the complete H₂O vapor pressure series of Bio-FHA coatings are presented in Fig. 4. The results confirmed that the BE for the F_{1s} transition shifted slightly towards lower energies, from 685.05 to 684.69 eV, as the H₂O vapor pressure increased.

Note that the high BE (685.05 eV) of coatings deposited with reduced or null H₂O vapor pressure, when compared with the target (684.20 eV), could be attributable to a different compound, for instance CaF₂ [51]. Note also that hydroxyl groups from the H₂O vapor atmosphere are known to replace groups of PO₄^{−3}, F[−] or CO₃^{−2}.

Based on the FTIR, XRD and XPS results and the referenced literature, the composition of our Bio-FHA coatings—deposited by PLD at 0.35 and 0.45 mbar of H₂O vapor pressure onto a marine bioceramic of pyrolyzed enameloid shark teeth—can be defined as a hydrated and fluorinated carbonated hydroxyapatite.

The role of water vapor pressure in producing fluorinated carbonated hydroxyapatite by PLD can be summarized as follows:

1. The presence of a H₂O vapor atmosphere reduces the kinetic energy of the species, causing a slower deposit rate and enhancing the crystalline quality of the films.
2. A greater number of hydroxyl groups are available in the growth process, allowing the crystalline structure to stabilize more easily.
3. The presence of a H₂O vapor atmosphere allows an ion exchange between OH[−], PO₄^{−3}, F[−] or CO₃^{−2} groups.

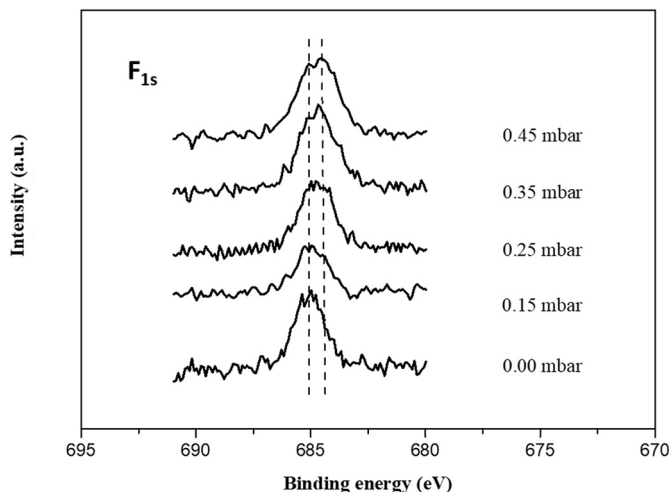


Fig. 4. High-resolution XPS spectra of F_{1s} electronic transition for the complete H₂O vapor pressure series of Bio-FHA coatings.

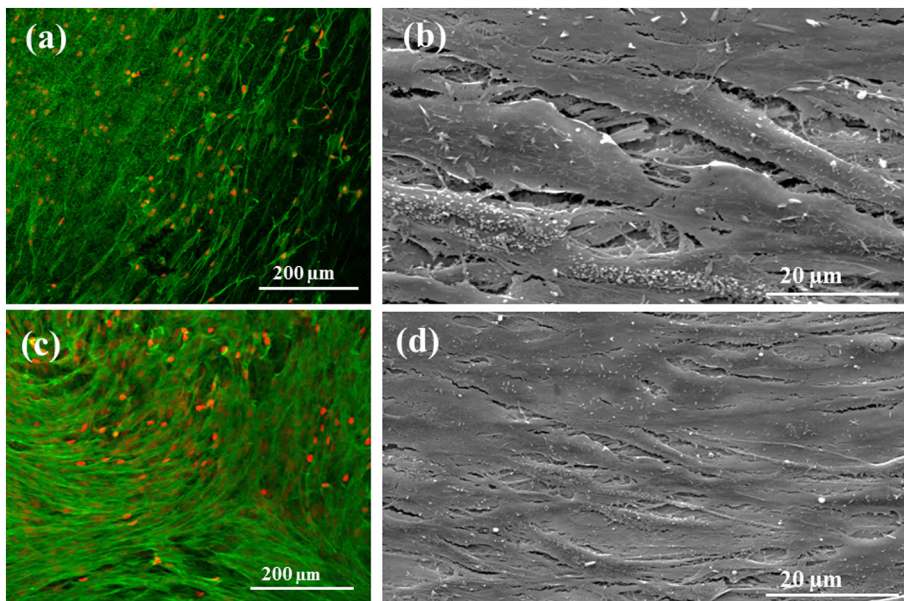


Fig. 5. Morphology of MC3T3-E1 cells on Bio-FHA (a, b) and Ref-HA (c, d) coatings, by CLSM (a, c) after 20 days of incubation, and by SEM (b, d) after 21 days of incubation. In the CLSM micrographs nuclei are stained in red and actin filaments in green. (For interpretation of the references to colour in this figure legend, the reader is referred to the web version of this article.)

- The main substitutions correspond to: (i) CO_3^{2-} ions for PO_4^{3-} and/or OH^- ions and (ii) F^- ions for OH^- ions
- The incorporation of F^- ions produces changes in the lattice structure of fluorinated carbonated hydroxyapatite coatings causing an increase in the crystal size and crystallinity [45].

3.2. Biological response: MC3T3-E1 pre-osteoblast viability

The Bio-FHA coatings processed at 0.45 mbar were selected for the biological evaluation, because of their proven crystallinity and good transference from the ablation target, including the incorporation of minority elements such as Na and Mg. Ref-HA coatings and TCP were also subjected to the experiments as material and experimental controls, respectively.

Fig. 5 presents the morphology of MC3T3-E1 cells on Bio-FHA (a, b) and Ref-HA (c, d) coatings, by CLSM (a, c) and by SEM (b, d). The cytoskeleton of the cell monolayers on both coatings stained in red (nuclei) and green (actin filaments) revealed a degree of elongation of actin filaments that appeared to be following the topography of the Bio-FHA coatings (a), as already depicted in Fig. 2. SEM of the same Bio-FHA coating (b) confirmed the typical flat morphology of cells that have formed a thick layer covering the entire coating. In the case of the Ref-HA coatings, the distribution of actin filaments forming a honeycomb-like structure is observed on the CLSM micrograph (c), and again a monolayer covering the entire coating (d) confirmed the healthy stage of cells.

Both coatings were proven to promote healthy morphology on the cells at the noted times of incubation; cells made contact with neighboring cells and covered the entire surface of their respective coatings (Bio-FHA and Ref-HA). The typical flat morphology of osteoblasts confirmed their healthy stage on both materials [50]. The morphology of the Bio-FHA coatings (Fig. 2), based on ridges and valleys following the direction of the topography of processed titanium substrates and composed of elongated structures of $< 1 \mu\text{m}$ in length, could contribute to the particular alignment observed in the cells' morphology. It is known from the literature that the topography strongly influences the morphology and functional activity of pre-osteoblasts, and that roughness favors osteogenic activity [59]. The literature has also reported on the orientation and aligned growth of osteoblasts on polymers or different ceramics [60, 61].

Cell proliferation was quantified after 7 and 21 days and results are presented in Fig. 6. After 7 days of incubation an intense proliferation of

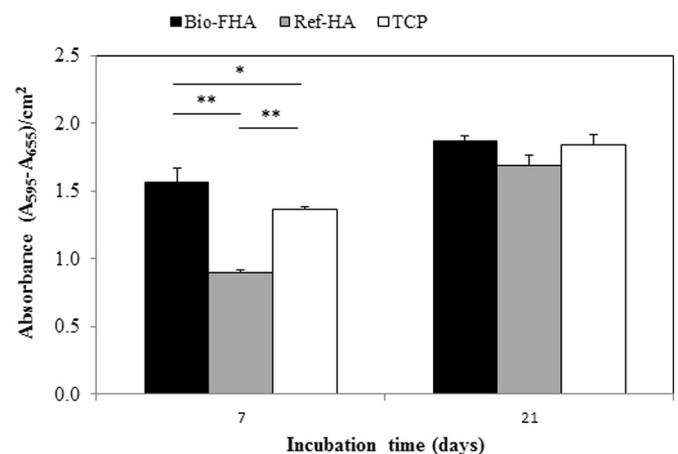


Fig. 6. MTT assay results after incubation of MC3T3-E1 pre-osteoblasts on Bio-FHA and Ref-HA coatings for 7 and 21 days. TCP was used as control. Data are presented as mean \pm standard error of the mean. Significant statistical differences for $p < 0.05$ (*) and $p < 0.01$ (**) are shown.

cells was observed on the Bio-FHA coatings; it was significantly higher ($p < 0.01$) than the proliferation on the Ref-HA coatings or the TCP control. After 21 days, all tested materials had higher values than on day 7, with both coatings at the same level as the TCPs. The proliferation values obtained for TCPs after both incubation periods of 7 and 21 days were as expected for this gold standard control. This control therefore confirms the healthy stage of cells throughout the experiment, and their good response when seeded on the two tested coatings at long periods of incubation.

Synthetic fluor-hydroxyapatite contributions on different materials have previously been tested in the literature, with good results in terms of proliferation, validating its non-cytotoxic behavior [1, 46, 52]. Biological fluorapatite obtained from shark enameloid has also performed well as granules and powder in in vitro tests [38]. Compared to these granules and powder, the Bio-FHA coatings in this study had compositional differences in terms of crystallinity, due to the processing conditions used to obtain them. Given the influence of H_2O vapor pressure demonstrated in this study, hydroxyl groups are thought to compete with PO_4^{3-} groups, promoting a Bio-FHA structure instead of Bio-FA (Fig. 4). The content of F (1.96 at.%), Na (0.95 at.%) and Mg (0.86 at.%) found in our Bio-FHA coatings resembled that of a previous

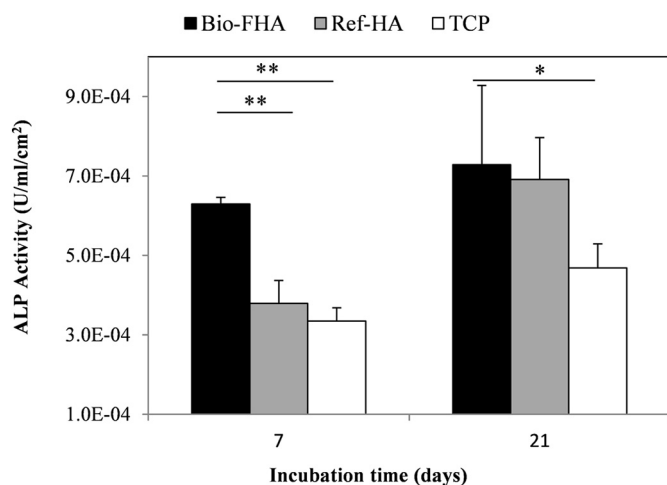


Fig. 7. ALP activity of MC3T3-E1 pre-osteoblasts on Bio-FHA and Ref-HA coatings, at 7 and 21 days. TCP was used as a control. Data are presented as mean \pm standard error of the mean. Significant statistical differences for $p < 0.05$ (*) and $p < 0.01$ (**) are shown.

study on bioceramics from shark teeth [37], where values were 1.0 ± 0.5 at.% for F, 0.90 ± 0.2 at.% for Na and 0.65 ± 0.04 at.% for Mg. These findings support the proven stoichiometric transference of the PLD methodology [16, 25]. These contributions could explain the intense osteoblastic proliferation on Bio-FHA coatings, compared to Ref-HA, after just 7 days of incubation (Fig. 6). The effect of fluoride on cell proliferation has previously been studied by Lau and Baylink [62], who demonstrated how fluoride contribution in concentrations of 0–30 μ M of fluoride increased bone cell proliferation.

Osteogenic activity of the MC3T3-E1 pre-osteoblasts on both coatings (Bio-FHA and Ref-HA) was evaluated by quantifying ALP activity at 7 and 21 days of incubation (Fig. 7). After 7 days of incubation, significant ALP activity ($p < 0.01$) was quantified on the Bio-FHA coatings compared to both the Ref-HA and TCP, which presented lower values in the same range. After 21 days of incubation, ALP activity increased in mean values on the two coatings and the TCP controls. However, the Bio-FHA and Ref-HA coatings showed higher levels of ALP activity ($p < 0.05$) than the TCP values. These results demonstrate the effective promotion of osteogenic activity by MC3T3-E1 pre-osteoblasts when seeded on Bio-FHA coatings after 7 and 21 days of incubation. The structure and morphology of fluor-hydroxyapatite, along with the contributions of F and minority elements Na and Mg, seemed to accelerate osteogenic activity.

In keeping with these results, several authors have previously reported on the promotion of cell proliferation and differentiation processes by synthetic FHA coatings [1, 46]. The differentiation of dental pulp stem cells and mesenchymal stem cells (MSCs) into osteoblasts was also observed on synthetic fluorapatite surfaces, where cells were able to successfully differentiate and mineralize [2, 54, 63, 64]. Ellingsen et al. [2] concluded that the presence of fluorine could contribute to bone healing and regeneration by inducing the differentiation of undifferentiated precursor cells into osteoblasts. In our case, the osteogenic activity of MC3T3-E1 pre-osteoblasts was already quantified at 7 days of incubation.

3.3. Biological response: antibacterial properties

To evaluate the antibacterial activity of the Bio-FHA and Ref-HA coatings, adhesion and biofilm formation were analyzed after incubation with *S. aureus* and *S. epidermidis*. The adhesion of both strains was first evaluated by SEM analysis and the results are displayed in Fig. 8, where micrographs (a, b) correspond to Bio-FHA and (c, d) to Ref-HA coatings; micrographs (a, c) relate to *S. epidermidis* and (b, d) to *S.*

aureus. Cocci, diplococci (white arrows) and aggregates were detected on both coatings. The presence of aggregates was observed especially on *S. aureus* (b, d). A slightly higher density of bacteria was detected on the Ref-HA coatings compared to the Bio-FHA (white squares).

The median number of CFUs for each coating and both bacterial strains was quantified after 24 h at 37 °C. As illustrated in Fig. 9, the adherence of *S. aureus* was significantly higher ($p < 0.05$) than *S. epidermidis* in both coatings. For *S. aureus*, there was a significant 3.6-fold reduction in biofilm formation on Bio-FHA (\log_{10} CFU/cm² = 8.11) compared to Ref-HA (\log_{10} CFU/cm² = 8.67) ($p = 0.0425$). In the case of *S. epidermidis*, the results showed a significant 2.4-fold reduction in biofilm formation on Bio-FHA (\log_{10} CFU/cm² = 6.87) compared to Ref-HA (\log_{10} CFU/cm² = 7.25) ($p = 0.0248$).

These results were in keeping with previous studies that have demonstrated the antibacterial effect of fluorine against oral bacteria [4–10]. In our research, the 1.96 at.% of fluorine was proven to be significantly effective against the species of bacteria responsible for 77% of infections in prosthetic implants. The contributions of other minority elements as a result of the biological origin of the target, together with the globular morphology and crystalline structure of the Bio-FHA coatings after PLD processing at 0.45 mbar of H₂O vapor pressure, contributed to the proliferation and differentiation of MC3T3-E1 pre-osteoblasts and kept the antibacterial properties of fluorine intact.

4. Conclusions

This study demonstrated both the feasibility of producing PLD coatings (Bio-FHA) from shark tooth enameloid in a H₂O vapor atmosphere and good compositional transference from the original bioceramic. It also showed how the coatings' composition and crystalline structure depended on the H₂O vapor pressures applied during the process. Increased pressure meant increased crystallinity: at the highest pressure of 0.45 mbar, more defined bands attributed to apatite diffraction planes, and crystallite sizes of up to 65 nm were detected. Higher pressures also resulted in a more efficient compositional transference from the target (even minority elements such as Na and Mg were transferred, in addition to Ca, P and F), the incorporation of carbonate groups and H₂O to the composition and, as a consequence, a decrease in the Ca/P ratio to values of around 1.8. When processed at 0.35–0.45 mbar, the original fluorapatite (with small contributions of tricalcium bis(orthophosphate) and/or whitlockite) of the shark tooth enameloid became a hydrated fluorinated carbonated hydroxyapatite. Compared to the synthetic hydroxyapatite coatings, the composition of the Bio-FHA coatings processed at 0.45 mbar, as well as the globular morphology of ridges, valleys and elongated structures of < 1 μ m in length, were shown to significantly ($p < 0.01$) favor the proliferation and ALP synthesis of MC3T3-E1 pre-osteoblasts after a short period. At the same time, it was demonstrated that the 1.96 at.% of F promoted a significant reduction in biofilm formation ($p < 0.05$) by *S. aureus* and *S. epidermidis*. These results confirmed the antibacterial properties of the Bio-FHA coatings, their in vitro biocompatibility in terms of proliferation and differentiation of MC3T3-E1 pre-osteoblasts, and their great potential for biomedical applications.

Acknowledgements

This research was partially supported by 0245 IBEROS1E and 0302 CVMARIIP, both from the INTERREG V Spain-Portugal (POCTEP) program; and Competitive Reference Groups (GRC) ED431C 2017_51 and Research networks ED431D 2017/13 both from the Xunta de Galicia, Spain. Hidalgo-Robatto B. M. acknowledges funding support from Xunta de Galicia pre-doctoral grant (A-2014). Technical support from CACTI (Universidade de Vigo) and J. Dorado are also gratefully acknowledged.

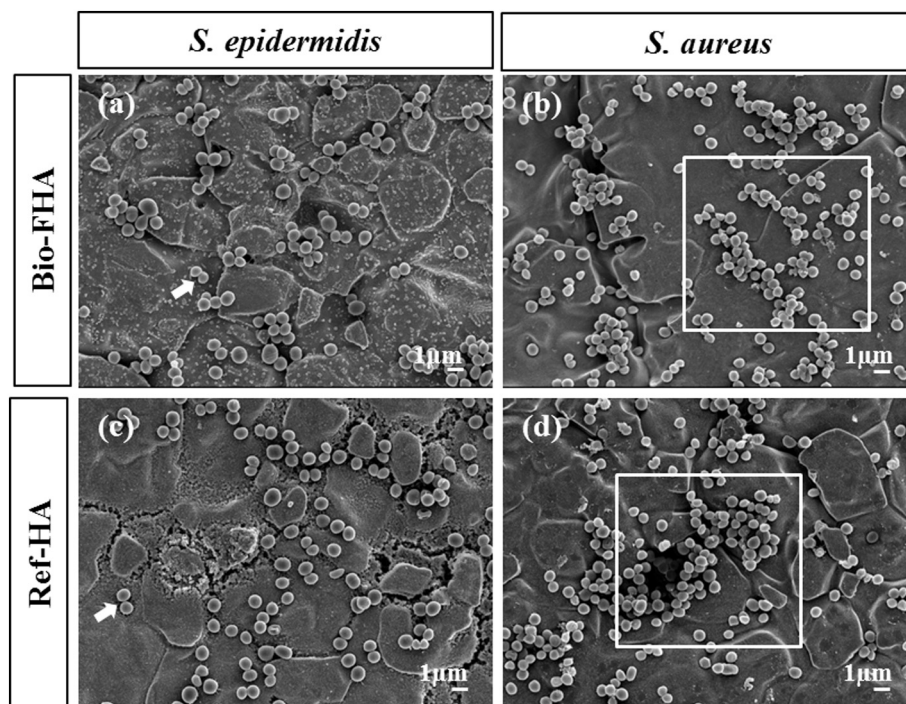


Fig. 8. SEM micrographs of *S. epidermidis* (a, c) and *S. aureus* (b, d) on Bio-FHA (a, b) and Ref-HA (c, d) coatings. White arrows indicate diplococci and white squares indicate areas with aggregates.

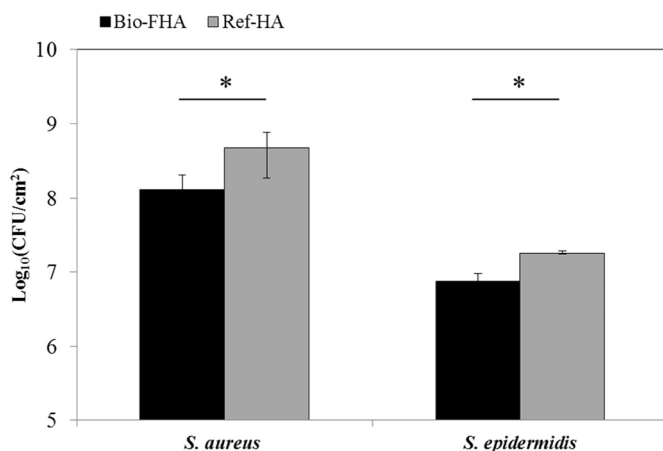


Fig. 9. $\text{Log}_{10}(\text{CFU}/\text{cm}^2)$ of *S. aureus* and *S. epidermidis* on Bio-FHA and Ref-HA coatings. Data are presented as median and interquartile range. Significant statistical differences for $p < 0.05$ (*) are shown.

Appendix A. Supplementary data

Supplementary data to this article can be found online at <https://doi.org/10.1016/j.surfcoat.2018.06.047>.

References

- [1] P. Yin, F.F. Feng, T. Lei, X.H. Zhong, X.C. Jian, Osteoblastic cell response on biphasic fluorhydroxyapatite/strontium-substituted hydroxyapatite coatings, *J. Biomed. Mater. Res. A* 102 (2014) 621–627.
- [2] J.E. Ellingsen, P. Thomsen, S.P. Lyngstadaas, S. Petter Lyngstadaas, Advances in dental implant materials and tissue regeneration, *Periodontol.* 2000 41 (2006) 136–156.
- [3] L. Gineste, M. Gineste, X. Ranz, A. Ellefterion, A. Guilhem, N. Rouquet, P. Frayssinet, Degradation of hydroxyapatite, fluorapatite, and fluorhydroxyapatite coatings of dental implants in dogs, *J. Biomed. Mater. Res.* 48 (1999) 224–234.
- [4] P.C. Baehni, Y. Takeuchi, Anti-plaque agents in the prevention of biofilm-associated oral diseases, *Oral Dis.* 9 (Suppl. 1) (2003) 23–29.
- [5] D.J. Bradshaw, P.D. Marsh, R.J. Hodgson, J.M. Visser, Effects of glucose and fluoride on competition and metabolism within in vitro dental bacterial communities and biofilms, *Caries Res.* 36 (2002) 81–86.
- [6] I.R. Hamilton, Biochemical effects of fluoride on oral bacteria, *J. Dent. Res.* 69 (1990) 660–667.
- [7] K. Nakajo, S. Imazato, Y. Takahashi, W. Kiba, S. Ebisu, N. Takahashi, Fluoride released from glass-ionomer cement is responsible to inhibit the acid production of caries-related oral streptococci, *Dent. Mater.* 25 (2009) 703–708.
- [8] H.M. Kay, M. Wilson, The in vitro effects of amine fluorides on plaque bacteria, *J. Periodontol.* 59 (1988) 266–269.
- [9] R.R. Mayhew, L.R. Brown, Comparative effect of SnF_2 , NaF, and SnCl_2 on the growth of *Streptococcus mutans*, *J. Dent. Res.* 60 (1981) 1809–1814.
- [10] S. Shani, M. Friedman, D. Steinberg, The anticariogenic effect of amine fluorides on *Streptococcus sobrinus* and glucosyltransferase in biofilms, *Caries Res.* 34 (2000) 260–267.
- [11] G.K. Wilcock, Benefits of total hip replacement to older patients and the community, *Br. Med. J.* 2 (1978) 37–39.
- [12] J.L. Del Pozo, M.S. Rouse, G. Euba, C.-I. Kang, J.N. Mandrekar, J.M. Steckelberg, R. Patel, The electrical effect is active in an experimental model of *Staphylococcus epidermidis* chronic foreign body osteomyelitis, *Antimicrob. Agents Chemother.* 53 (2009) 4064–4068.
- [13] Y. Abu-Amer, I. Darweh, J.C. Clohisy, Aseptic loosening of total joint replacements: mechanisms underlying osteolysis and potential therapies, *Arthritis Res. Ther.* 9 (2007) S6.
- [14] P. Piscitelli, G. Iolascon, M. Innocenti, R. Civinini, A. Rubinacci, M. Muratore, M. D'Arienzo, P.T. Leali, A.M. Carossino, M.L. Brandi, Painful prosthesis: approaching the patient with persistent pain following total hip and knee arthroplasty, *Clin. Cases Miner. Bone Metab.* 10 (2013) 97–110.
- [15] R. Narayanan, S.K. Seshadri, T.Y. Kwon, K.H. Kim, Calcium phosphate-based coatings on titanium and its alloys, *J. Biomed. Mater. Res. Part B Appl. Biomater.* 85B (2008) 279–299.
- [16] B. León, J.J.A. León, Betty, Pulsed laser deposition of thin calcium phosphate coatings, *Thin Calcium Phosphate Coatings for Medical Implants*, Springer New York, New York, 2009, pp. 101–156.
- [17] M. Manzano, M. Vallet-Regí, Revisiting bioceramics: bone regenerative and local drug delivery systems, *Prog. Solid State Chem.* 40 (2012) 17–30.
- [18] Q. Bao, J. Zhang, The effect of Y_2O_3 on properties of hydroxyapatite thin films prepared by pulsed laser deposition, *J. Biomimetics, Biomater. Biomed. Eng.* 29 (2016) 22–32.
- [19] N. Fujita, T. Makino, Y. Sakoishi, K. Asano, M. Kusunoki, Pulsed laser deposition of pure fluoroapatite film without OH groups, *Cryst. Res. Technol.* 51 (2016) 215–219.
- [20] B.M. Hidalgo-Robatto, M. López-Álvarez, A.S. Azevedo, J. Dorado, J. Serra, N.F. Azevedo, P. González, Pulsed laser deposition of copper and zinc doped hydroxyapatite coatings for biomedical applications, *Surf. Coat. Technol.* 333 (2018) 168–177.
- [21] A. Janković, S. Eraković, C. Ristoscu, N. Mihailescu Serban, L. Duta, A. Visan, G.E. Stan, A.C. Popa, M.A. Husanu, C.R. Luculescu, V.V. Srdić, D. Janačković, V. Mišković-Stanković, C. Bleotu, M.C. Chifiriuc, I.N. Mihailescu, Structural and biological evaluation of lignin addition to simple and silver-doped hydroxyapatite

- thin films synthesized by matrix-assisted pulsed laser evaporation, *J. Mater. Sci. Mater. Med.* 26 (2015) 5333.
- [22] N. Mihailescu, G.E. Stan, L. Duta, M.C. Chifiriuc, C. Bleotu, M. Sopronyi, C. Luculescu, F.N. Oktar, I.N. Mihailescu, Structural, compositional, mechanical characterization and biological assessment of bovine-derived hydroxyapatite coatings reinforced with MgF₂ or MgO for implants functionalization, *Mater. Sci. Eng. C* 59 (2016) 863–874.
- [23] J.V. Rau, I. Cacciotti, S. Laureti, M. Fosca, G. Varvaro, A. Latini, Bioactive, nanostructured Si-substituted hydroxyapatite coatings on titanium prepared by pulsed laser deposition, *J Biomed Mater Res B Appl Biomater* 103 (2015) 1621–1631.
- [24] C. Rodríguez-Valencia, P. Freixeiro, J. Serra, C.M. Ferreirós, P. González, M. López-Álvarez, In vitro evaluation of the antibacterial and osteogenic activity promoted by selenium-doped calcium phosphate coatings, *Biomed. Mater.* 12 (2017) 15–28.
- [25] E.L. Solla, P. González, J. Serra, S. Chiussi, B. León, J.G. López, Pulsed laser deposition of silicon substituted hydroxyapatite coatings from synthetic and biological sources, *Appl. Surf. Sci.* 254 (2007) 1189–1193.
- [26] A.J. Tande, D.R. Osmon, K.E. Greenwood-Quaintance, T.M. Mabry, A.D. Hanssen, R. Patel, Clinical characteristics and outcomes of prosthetic joint infection caused by small colony variant staphylococci, *MBio* 5 (2014) e01910-14.
- [27] N. Benito, M. Franco, A. Ribera, A. Soriano, D. Rodríguez-Pardo, L. Sorlí, G. Fresco, M. Fernández-Sampedro, M. Dolores del Toro, L. Guío, E. Sánchez-Rivas, A. Bahamonde, M. Riera, J. Esteban, J.M. Baraia-Etxaburu, J. Martínez-Alvarez, A. Jover-Sáenz, C. Dueñas, A. Ramos, B. Sobrino, G. Euba, L. Morata, C. Pigrau, P. Coll, I. Mur, J. Ariza, F. Barcenilla, F. Pérez-Villar, L. Prats-Gispert, R. Cisterna, S. Ibarra, J.M. Santamaría López, J. Cabo, D. García, J. Lora-Tamayo, O. Murillo, S. Pedrero, S. Álvarez-Parrondo, R. Muedra-Font, C. Raya-Fernández, C. Rodríguez-Alonso, A. Moreno, M.A. Blanco-Martínez-de-Morentin, R. Cabo-Magadan, A. Combalia, S. García, J.C. Martínez-Pastor, E. Tornero, J. Merino-Pérez, J.M. Montejo, A. Alier, J.P. Horcajada, V. Plasencia, L. Puig, A. Blanco Añón, J. García-Cañete, E. Sandoval, M. Fakkas-Fernández, C. Garcés-Zarzalejo, C. Fariñas-Alvarez, M.C. Fariñas, L. Martínez-Martínez, C. Salas-Venero, J. Cobo, P. Ruiz-Carbajosa, M. Jordán, X. Crusi, C. Marinescu, F. Montaner, A. Ramírez, P.S. Corona, M. Lung, M. Muniain-Ezcurra, C. Peñas-Espinar, A.I. Suárez, R. Álvarez, J.A. Cordero, M. López-Pliego, J. Palomino, A. Puente, Time trends in the aetiology of prosthetic joint infections: a multicentre cohort study, *Clin. Microbiol. Infect.* 22 (2016) 732.e1–732.e8.
- [28] P.L. Tran, A.A. Hammond, T. Mosley, J. Cortez, T. Gray, J.A. Colmer-Hamood, M. Shashtri, J.E. Spallholz, A.N. Hamood, T.W. Reid, Organoselenium coating on cellulose inhibits the formation of biofilms by *Pseudomonas aeruginosa* and *Staphylococcus aureus*, *Appl. Environ. Microbiol.* 75 (2009).
- [29] J. Barros, L. Grenho, C.M. Manuel, C. Ferreira, L. Melo, O.C. Nunes, F.J. Monteiro, M.P. Ferraz, Influence of nanohydroxyapatite surface properties on *Staphylococcus epidermidis* biofilm formation, *J. Biomater. Appl.* 28 (2014) 1325.
- [30] M. Ribeiro, F.J. Monteiro, M.P. Ferraz, Infection of orthopedic implants with emphasis on bacterial adhesion process and techniques used in studying bacterial-material interactions, *Biomater.* 2 (2012) 176–194.
- [31] E.M. Hetrick, M.H. Schoenfish, Reducing implant-related infections: active release strategies, *Chem. Soc. Rev.* 35 (2006) 780–789.
- [32] E. Boanini, M. Gazzano, A. Bigi, Ionic substitutions in calcium phosphates synthesized at low temperature, *Acta Biomater.* 6 (2010) 1882–1894.
- [33] E.L. Solla, B. Rodríguez-González, H. Aguiar, C. Rodríguez-Valencia, J. Serra, P. González, Revealing the nanostructure of calcium phosphate coatings using HRTEM/FIB techniques, *Mater. Character.* 122 (2016) 148–153.
- [34] I. Pereiro, C. Rodríguez-Valencia, C. Serra, E.L. Solla, J. Serra, P. González, Pulsed laser deposition of strontium-substituted hydroxyapatite coatings, *Appl. Surf. Sci.* 258 (2012) 9192–9197.
- [35] E.L. Solla, J.P. Borrajo, P. González, J. Serra, S. Chiussi, B. León, J.G. López, Study of the composition transfer in the pulsed laser deposition of silicon substituted hydroxyapatite thin films, *Appl. Surf. Sci.* 253 (2007) 8282–8286.
- [36] H. Aguiar, S. Chiussi, M. López-Álvarez, P. González, J. Serra, Structural characterization of bioceramics and mineralized tissues based on Raman and XRD techniques, *Ceram. Int.* 44 (2018) 495–504.
- [37] M. López-Álvarez, E. Vigo, C. Rodríguez-Valencia, V. Outeiriño-Iglesias, P. González, J. Serra, In vivo evaluation of shark teeth-derived bioapatites, *Clin. Oral Implants Res.* 28 (2017) 91–100.
- [38] M. López-Álvarez, S. Pérez-Davila, C. Rodríguez-Valencia, P. González, J. Serra, The improved biological response of shark tooth bioapatites in a comparative in vitro study with synthetic and bovine bone grafts, *Biomed. Mater.* 11 (3) (2016) 035011(1–13).
- [39] J. Esteban, E. Gomez-Barrena, J. Cordero, N.Z. Martín-de-Hijas, T.J. Kinnari, R. Fernandez-Roblas, Evaluation of quantitative analysis of cultures from sonicated retrieved orthopedic implants in diagnosis of orthopedic infection, *J. Clin. Microbiol.* 46 (2008) 488–492.
- [40] B. Herigstad, M. Hamilton, J. Heersink, How to optimize the drop plate method for enumerating bacteria, *J. Microbiol. Methods* 44 (2001) 121–129.
- [41] J.M. Hughes, M. Cameron, K.D. Crowley, Structural variations in natural F, OH, and Cl apatites, *Am. Mineral.* 74 (1989) 870–876.
- [42] A. Joseph Nathanael, D. Mangalaraj, S.I. Hong, Y. Masuda, Y.H. Rhee, H.W. Kim, Influence of fluorine substitution on the morphology and structure of hydroxyapatite nanocrystals prepared by hydrothermal method, *Mater. Chem. Phys.* 137 (2013) 967–976.
- [43] J.L. Arias, F.J. García-Sanz, M.B. Mayor, S. Chiussi, J. Pou, B. León, M. Pérez-Amor, Physicochemical properties of calcium phosphate coatings produced by pulsed laser deposition at different water vapour pressures, *Biomaterials* 19 (1998) 883–888.
- [44] R.K. Singh, F. Qian, V. Nagabushnam, R. Damodaran, B.M. Moudgil, Excimer laser deposition of hydroxyapatite thin films, *Biomaterials* 15 (1994) 522–528.
- [45] J.H. Shepherd, D.V. Shepherd, S.M. Best, Substituted hydroxyapatites for bone repair, *J. Mater. Sci. Mater. Med.* 23 (2012) 2335–2347.
- [46] B.D. Hahn, Y.L. Cho, D.S. Park, J.J. Choi, J. Ryu, J.W. Kim, C.W. Ahn, C. Park, H.E. Kim, S.G. Kim, Effect of fluorine addition on the biological performance of hydroxyapatite coatings on Ti by aerosol deposition, *J. Biomater. Appl.* 27 (2013) 587–594.
- [47] A. Forghani, M. Mapar, M. Kharaziha, M.H. Fathi, M. Fesharaki, Novel fluorapatite-forsterite nanocomposite powder for oral bone defects, *Int. J. Appl. Ceram. Technol.* 10 (2013) 282–289.
- [48] R.Z. Legeros, L.M. Silverstone, G. Daculsi, L.M. Kerebel, In vitro caries-like lesion formation in F-containing tooth enamel, *J. Dent. Res.* 62 (1983) 138–144.
- [49] M. Kheradmandfar, M.H. Fathi, F. Ansari, T. Ahmadi, Effect of mg content on the bioactivity and biocompatibility of Mg-substituted fluorapatite nanopowders fabricated via mechanical activation, *Mater. Sci. Eng. C* 68 (2016) 136–142.
- [50] C. Rodríguez-Valencia, I. Pereiro, R.P. Pirrao, M. López-Álvarez, J. Serra, P. González, A.P. Marques, R.L. Reis, Human mesenchymal stem cells response to multi-doped silicon-strontium calcium phosphate coatings, *J. Biomater. Appl.* 28 (2014) 1397–1407.
- [51] K.J. Roche, K.T. Stanton, Measurement of fluoride substitution in precipitated fluorhydroxyapatite nanoparticles, *J. Fluor. Chem.* 161 (2014) 102–109.
- [52] K.A. Bhadang, K.A. Gross, Influence of fluorapatite on the properties of thermally sprayed hydroxyapatite coatings, *Biomaterials* 25 (2004) 4935–4945.
- [53] J. Wei, J. Wang, W. Shan, X. Liu, J. Ma, C. Liu, J. Fang, S. Wei, Development of fluorapatite cement for dental enamel defects repair, *J. Mater. Sci. Mater. Med.* 22 (2011) 1607–1614.
- [54] Y.F. Niu, L.H. Cao, J. Wei, Y.H. Ma, S.J. Song, W.Z. Weng, H.H. Li, C.S. Liu, J.C. Su, Development of a bioactive composite of nano fluorapatite and poly(butylene succinate) for bone tissue regeneration, *J. Mater. Chem. B* 2 (2014) 1174–1181.
- [55] N. Iqbal, M.R. Abdul Kadir, N.H. Bin Mahmood, S. Iqbal, D. Almasi, F. Naghizadeh, H.R. Balaji, T. Kamarul, Characterization and biological evaluation of silver containing fluorapatite nanoparticles prepared through microwave synthesis, *Ceram. Int.* 41 (2015) 6470–6477.
- [56] J. Liu, S.C.F. Rawlinson, R.G. Hill, F. Fortune, Fluoride incorporation in high phosphate containing bioactive glasses and in vitro osteogenic, angiogenic and antibacterial effects, *Dent. Mater.* 32 (2016) 221–237.
- [57] H. Toktamış, D. Toktamış, S.M. Yılmaz, A.N. Yazici, S. Yildirim, Ö. Özbiçki, The investigation of usage of fluorapatite mineral (Ca₅F(PO₄)₃) in tooth enamel under the different pre-irradiation thermal treatments, *Thermochim. Acta* 600 (2015) 102–109.
- [58] K. Cheng, S. Zhang, W. Weng, Surface characterization of colloidal-sol gel derived biphasic HA/FA coatings, *J. Mater. Sci. Mater. Med.* 18 (2007) 2011–2015.
- [59] E. Martínez, E. Engel, J.A. Planell, J. Samitier, Effects of artificial micro- and nano-structured surfaces on cell behaviour, *Ann. Anat.* 191 (2009) 126–135.
- [60] D. Cordero, M. López-Álvarez, C. Rodríguez-Valencia, J. Serra, S. Chiussi, P. González, In vitro response of pre-osteoblastic cells to laser microgrooved PEEK, *Biomed. Mater.* 8 (2013) 055006.
- [61] M. López-Álvarez, I. Pereiro, J. Serra, A. De Carlos, P. González, Osteoblast-like cell response to macro- and micro-patterned carbon scaffolds obtained from the sea rush *Juncus maritimus*, *Biomed. Mater.* 6 (2011) 045012.
- [62] K.H. Lau, D.J. Baylink, Molecular mechanism of action of fluoride on bone cells, *J. Bone Miner. Res.* 13 (1998) 1660–1667.
- [63] X. Wang, T. Jin, S. Chang, Z. Zhang, A. Czajka-Jakubowska, J.E. Nör, B.H. Clarkson, L. Ni, J. Liu, In vitro differentiation and mineralization of dental pulp stem cells on enamel-like fluorapatite surfaces, *Tissue Eng. Part C Methods* 18 (2012) 821–830.
- [64] J. Liu, T. Jin, S. Chang, A. Czajka-Jakubowska, Z. Zhang, J.E. Nör, B.H. Clarkson, The effect of novel fluorapatite surfaces on osteoblast-like cell adhesion, growth, and mineralization, *Tissue Eng. Part A* 16 (2010) 2977–2986.